Editors' Suggestion

Black Holes as Telescopes: Discovering Supermassive Binaries through Quasiperiodic Lensed Starlight

Hanxi Wang [*]
Department of Physics, Astrophysics, University of Oxford, Denys Wilkinson Building, Keble Road, Oxford, OX1 3RH, United Kingdom

Miguel Zumalacárregui [†]
Max Planck Institute for Gravitational Physics (Albert Einstein Institute), Am Mühlenberg 1, D-14476 Potsdam-Golm, Germany

Bence Kocsis [‡]
Rudolf Peierls Centre for Theoretical Physics, University of Oxford, Clarendon Laboratory, Parks Road, Oxford, OX1 3PU, United Kingdom and St Hugh's College, University of Oxford, St Margaret's Road, Oxford, OX2 6LE, United Kingdom

(Received 10 July 2025; accepted 2 December 2025; published 12 February 2026)

Supermassive black hole (SMBH) binary systems are an unavoidable outcome of galaxy mergers. Their dynamics encode valuable information about their formation and growth, the composition of their host galactic nuclei, the evolution of galaxies, and the nature of gravity. Many SMBH binaries with separations pc-kpc have been found, but closer (subparsec) binaries remain to be confirmed. Identifying these systems may elucidate how binaries evolve past the "final parsec" until gravitational radiation drives them to coalescence. Methods to discover and characterize SMBH binaries can shed light on these important questions and potentially open new multimessenger channels. Here we show that SMBH binaries in nonactive galactic nuclei can be identified and characterized by the gravitational lensing of individual bright stars, located behind them in the host galaxy. The rotation of "caustics"—regions where sources are hugely magnified due to the SMBH binary's orbit and inspiral—leads to quasiperiodic lensing of starlight (QPLS). The extreme lensing magnification of individual bright stars produces a significant variation in the host galaxies' luminosity; their lightcurve traces the orbit of the SMBH binary and its evolution, analogous to the waveforms recorded by gravitational-wave (GW) detectors. QPLS probes the population of sources observable by pulsar timing arrays and space detectors (LISA, TianQin), offering advance warning triggers for merging SMBHs for coincident or follow-up GW detections. SMBH population models predict 1–50 [190–5000]$(n_\star/\mathrm{pc}^{-3})$ QPLS binaries with period less than 10[40] yr with comparable masses and redshift $z < 0.3$, where $n_\star$ is the stellar number density. Additionally, stellar and orbital motion will lead to frequent instances of single or double flares caused by SMBHBs with longer periods. This novel signature can be searched for in a wealth of existing and upcoming time-domain photometric data: identifying quasiperiodic variability in galactic lightcurves will reveal an ensemble of binary systems and illuminate outstanding questions around them.

DOI: 10.1103/1sfl-87t4

Introduction—Astronomical observations demonstrate that most galaxies harbor a supermassive black hole (SMBH) at their center. As galaxies merge, their central black holes encounter each other, forming bound systems. The evolution of these systems is driven by interactions with the surrounding star cluster, gaseous drag, and the emission of gravitational radiation [1–3]. Identifying SMBH binary (SMBHB) systems will elucidate interactions between central black holes and galactic nuclei (Refs. [4,5] p. 81, Fig. 17), their role in galaxy formation and evolution [6,7], and provide new tests of gravity and fundamental physics [8,9]. Many SMBHBs with parsec (pc) to kiloparsec (kpc) separation have been identified [10]. Candidates for tighter binaries with subparsec separation need to be confirmed [11].

[*]Contact author: hanxi.wang@physics.ox.ac.uk
[†]Contact author: miguel.zumalacarregui@aei.mpg.de
[‡]Contact author: bence.kocsis@physics.ox.ac.uk

Published by the American Physical Society under the terms of the Creative Commons Attribution 4.0 International license. Further distribution of this work must maintain attribution to the author(s) and the published article's title, journal citation, and DOI.

Tight, sub-pc SMBHBs evolve via gravitational wave (GW) emission, opening the possibility of multimessenger observations if coincident GW and electromagnetic (EM) emission is identified [9,12,13]. Building evidence for a nanoHz GW background using pulsar timing arrays (PTA) [14–17] sheds light on the population of binaries with mass $\gtrsim 10^8 M_\odot$ [18,19]. Spaceborne GW detectors in the mHz band, LISA [20,21], and TianQin [22,23], will record mergers of binaries 10^5–$10^8 M_\odot$ and open new windows into astrophysics and cosmology [5,24].

Identifying tight SMBHBs with EM observations is challenging. Most methods require the SMBHB to be embedded in gas and shine as a bright active galactic nucleus (AGN), and rely on detecting modulations of the emission of the accreted gas, where the binary motion imprints regular features modulated by the orbital period due to, e.g., gravitational torques, accretion variability, or relativistic Doppler boost [25–29]. SMBHBs can also be discovered by gravitational lensing, the deflection and magnification of light signals by gravitational fields [30,31]. One possibility is the lensing of a black hole's accretion disk by its companion, potentially leading to periodic flares [32–35], or the lensing of blazar jets by an intervening intermediate mass black hole binary [36]. Other studies consider the effect of SMBHBs on central images in galaxy-galaxy lenses, whose faint modulations may be detectable [37,38]. To the best of our knowledge the lensing effect of SMBHBs on individual stars in the host galaxy remains unexplored.

Here we demonstrate how SMBHBs can act as telescopes, magnifying individual stars' brightness comparable to their host galaxy: the orbital motion generates quasi-periodic lensing of starlight (QPLS), a characteristic time-dependent photometric lightcurve revealing the SMBHB's presence and dynamics. This method bears resemblance to microlensing by binary stars or by exoplanets, where the light of a star in the Milky Way is lensed by a star-planet binary system crossing the line of sight: this imprint reveals the binary properties [39–41]. For QPLS, the source magnification can be much higher than in exoplanet searches, and even surpass highly amplified individual stars found in giant arcs of galaxy clusters [42–44]. Note that this method does not require gas to be present around the SMBHBs, which may be an advantage given that more than 90% of galaxies do not produce an AGN [45].

The likelihood of lensing by an inspiraling SMBHB is greatly increased compared to a static lens. The changing position and separation of the binary increases the solid angle of source directions affected by lensing. The caustic curve of the SMBHB lens rotates and slowly shrinks with the inspiraling binary's orbit, it crosses the image of the star repeatedly, and creates a quasiperiodic light curve. The timing and shape of this QPLS lightcurve carries information on the mass, period, inclination, and eccentricity of the SMBHB.

High magnification by binary lenses—We model the SMBHB as a two-point-mass lens [46]. The lenses have mass M_1 and M_2 and we approximate them as projected to a common lens plane (perpendicular to the line of sight) at an angular diameter distance $D_{\rm L}$ from the observer. The source is a star in the same galaxy as the SMBHB, whose distance to the observer (D_S) and to the lens plane ($D_{\rm LS}$) satisfy $D_{\rm LS} \ll D_{\rm L} \sim D_S$. The Einstein radius of this system corresponds to a distance

$$\xi_0 = 2\sqrt{R_{\rm g}\frac{D_L D_{\rm LS}}{D_S}} \approx 2\sqrt{R_{\rm g} D_{\rm LS}} = 1.38\,{\rm pc} M_{10}^{1/2} D_{\rm kpc}^{1/2}, \quad (1)$$

where $R_{\rm g} = GM/c^2$, $M = M_1 + M_2$ is the total mass of the binary, $M_{10} = M/(10^{10} M_\odot)$, and $D_{\rm kpc} = D_{\rm LS}/{\rm kpc}$. The lens equation is expressed in units of the Einstein radius as

$$\boldsymbol{y} = \boldsymbol{x} - m_1 \frac{\boldsymbol{x} - \boldsymbol{x}_{m_1}}{|\boldsymbol{x} - \boldsymbol{x}_{m_1}|^2} - m_2 \frac{\boldsymbol{x} - \boldsymbol{x}_{m_2}}{|\boldsymbol{x} - \boldsymbol{x}_{m_2}|^2}, \quad (2)$$

where $(D_{\rm S}/D_{\rm L})\xi_0 \boldsymbol{y}$ is the source position in the source plane, $\xi_0 \boldsymbol{x}$ is the position of the image in the lens plane, $\xi_0 \boldsymbol{x}_{m_1}$ and $\xi_0 \boldsymbol{x}_{m_2}$ are the positions of the two point-mass lenses in the lens plane, and m_1 and m_2 are given by $m_{1,2} = M_{1,2}/(M_1 + M_2)$ (we will refer to source frame quantities, unless otherwise stated).

The magnification μ of an image is computed from the Jacobian of the lens equation, $\mu = \det(|\partial \boldsymbol{y}/\partial \boldsymbol{x}|)^{-1}$. Solving $\det(|\partial \boldsymbol{y}/\partial \boldsymbol{x}|) = 0$ for a point source gives the image positions at which the magnification diverges, which collectively form the *critical curves*. Mapping the critical curves to the source plane using the lens equation (2) defines the *caustic curves*. A point source on the caustic curve is expected to have infinite magnification. In practice, the maximum magnification is limited by the signal's wavelength and/or spatial size of the source. We refer the reader to Supplemental Material [47] for more details on the methods and assumptions used in the magnification calculation.

Evaluating the magnification as a superposition of pointlike emitters covering the stellar surface, we find that the SMBHB lenses are able to magnify a star in the host galaxy of radius 10–$10^3 R_\odot$ by a factor $\mu = 10^{4-6}$ [Eq. (3) below]. Bright sources, such as red giants or main-sequence O/B-type stars, have luminosities of $10^{2-6} L_\odot$, which can be amplified to $10^{6-12} L_\odot$, producing a potentially significant variability in the brightness of the entire host galaxy. In particular, given that massive O-type stars shine with the Eddington luminosity, $L_{\rm Edd} = 4\pi G c M_*/\kappa = 3.2 \times 10^6 L_\odot (M_*/100 M_\odot)$, where κ is the electron-scattering opacity, the luminosity variations of a lensed O-star match $L_{\rm Edd}$ of a SMBH with $M_\bullet = \mu M_* = 10^{7-8} M_\odot (M_*/100 M_\odot)$. Thus, bright stars lensed by quiescent SMBHBs devoid of gas produce a bright AGN, but

with distinct spectral signatures and predictable variability patterns.

The critical and caustic curves have three different topologies [46] based on $d \equiv |\boldsymbol{x}_{m_1} - \boldsymbol{x}_{m_2}|$, the dimensionless separation between the lenses projected into the lens plane. For eccentric binary lenses with semimajor axis a, eccentricity e, and orbital plane perpendicular to the line-of-sight to the observer, d varies between $(1+e)a/\xi_0$ (apocenter passage) and $(1-e)a/\xi_0$ (pericenter passage), where $a/\xi_0 = 0.0075 T_{\rm yr}^{2/3} M_{10}^{-1/6} D_{\rm kpc}^{-1/2}$ from Kepler's law, $T_{\rm yr}$ is the orbital period in units of yr. For quasicircular binary lenses with orbital plane inclination relative to the line of sight ι, d varies between a/ξ_0 and $a\cos\iota/\xi_0$.

Quasiperiodic lensing of starlight—We consider a static source with respect to the lenses' center-of-mass, and focus on cases with a face-on binary lens with respect to the observer at separation $d \ll 1$. In this case, the caustic curve has a diamond shape with maximum diameter $\xi_0 d^2$ centered on the center-of-mass of the lenses, as shown in Fig. 1. The corresponding critical curve is approximately a circle with radius $\approx\xi_0$ (the Einstein ring). Two additional caustic triangles form at distance $\sim\xi_0/d$ perpendicular to the binary axis (see Fig. S2 in Supplemental Material [47]). We will focus on the central diamond-shaped caustic, where the magnification is highest.

For a SMBHB on a circular orbit, the diamond-shaped caustic curve rotates rigidly around its center. The most prominent variability is obtained for a star situated within an annulus of inner and outer radii matching the innermost (fold) and outermost (cusp) points of the caustic, respectively. In this case, the caustic curve crosses the star multiple times during each period, resulting in high-magnification events eight times (near-fold crossing) or four times (near-cusp crossing) per period. A significant quasiperiodic modulation is obtained even without caustic crossing four times per orbit in cases when the star is just outside the caustic. If the SMBHB inspirals due to GW emissions, the separation between the lenses shrinks, causing the caustic curve to shrink as $\sim d^2\xi_0$ (see Supplemental Material [47] for details). Once the caustic is fully inside the star, the number of peaks and amplitude change in the light curve.

For an equal-mass binary, the magnifications for cusp and fold crossings are approximately between (see Supplemental Material [47] for more details)

$$\mu_{\rm cusp} \approx 1\times 10^6 (1\pm e)^{-0.7} M_{10}^{0.44} T_{\rm yr}^{-0.47} R_{10}^{-0.64} D_{\rm kpc}^{0.67}, \quad \text{and} \quad (3)$$

$$\mu_{\rm fold} \approx 4\times 10^5 (1\pm e)^{-1} M_{10}^{5/12} T_{\rm yr}^{-2/3} R_{10}^{-1/2} D_{\rm kpc}^{3/4}, \quad (4)$$

where e is the eccentricity, $R_{10} = R_{\rm src}/10R_\odot$ is the radius of the source in units of 10 solar radii, $D_{\rm kpc} = D_{\rm LS}/1$ kpc is the lens-source distance in units of kpc, and the $(1\pm e)$ dependence corresponds to caustic crossing near apastron and periastron passage, respectively. These estimates assume that the source diameter is smaller than the largest diameter of the caustic curve, i.e.,

$$R_{\rm src} \le \frac{1}{2}\xi_0 d^2 \approx 3500 R_\odot (1\pm e)^2 M_{10}^{1/6} T_{\rm yr}^{4/3} D_{\rm kpc}^{-1/2}. \quad (5)$$

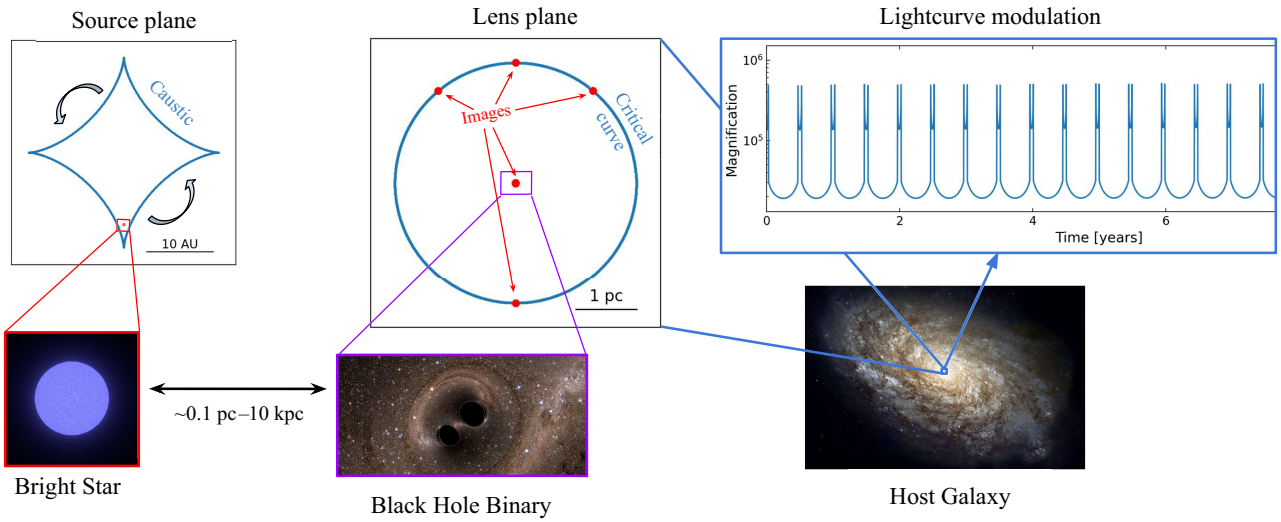


FIG. 1. Quasiperiodic lensing of starlight: a bright star (left) is highly magnified by a binary supermassive black hole binary (center). The caustic rotates as the binary orbits, producing a bright quasiperiodic signal at the central region of the host galaxy (right). The SMBHB in the diagram has total mass of $10^{10}M_\odot$ and an initial period of 2 years. The distance between the lens and source plane is 1 kpc, the star has a size of $10R_\odot$. The red dots in the lens plane mark the positions of the images. There are 5 (3) images when the source is inside (outside) the caustic curves, out of which 4 (2) images are near the critical curve hence highly magnified. In addition to the diamond-shaped caustic, two triangle-shaped caustics form at about 230 pc from the center of mass (not shown). Credit: NASA/ESA, SXS/AEI, ESO [70].

For larger sources, only a portion of their area is highly magnified, resulting in a reduced overall magnification and a reduced level of variabiliy due to caustic rotation.

The duration of peak brightening during caustic crossing is

$$t_{\rm mag} \approx 16\ {\rm hr}(1-e^2)^{-1/2} M_{10}^{-1/6} T_{\rm yr}^{-1/3} R_{10} D_{\rm kpc}^{1/2} \qquad (6)$$

for both apastron and periastron caustic crossing (see Supplemental Material [47] for more details).

We will now present two examples for which QPLS by an inspiraling SMBHB produces prominent photometric variability: a quasicircular SMBHB and an eccentric LISA binary. We will comment on the potential of these sources for multimessenger observations.

(1) Quasicircular merger and pulsar timing arrays. Figure 2 shows the QPLS magnification curve of a star of radius $10R_\odot$ in the host galaxy of an inspiraling quasicircular, face-on, equal-mass SMBHB with $10^{10}M_\odot$ component-mass binary lenses. The source star is fixed at a distance of 1 kpc behind the SMBHB lens, 5 A.U. off axis from the line of sight to the SMBHB center of mass in the source plane. The figure shows the flux magnification as a function of time to merger for the final 13 years of the inspiral before merger (the observed merger time is computed assuming the redshift of the host galaxy is $z = 0.5$). All the observed times and frequencies of the QPLS sources are evaluated at this redshift in the remaining main text. Insets show five representative snapshots of the caustic curve, which rotates counterclockwise with the orbital period of the SMBHB.

Magnification peaks occur when the caustic curve crosses the source, initially eight times per orbit, i.e., once every 2 months at 13 yrs to merger. Local minima occur when the source distance from the caustic has a maximum, i.e., when the source is aligned with the innermost points of the caustic (i.e., with the innermost fold, see Fig. 2 in Supplemental Material [47]). As the SMBH inspirals, the caustic curve shrinks in size (see insets). The light curve changes from fold crossing to cusp crossing producing the largest magnification $\mu_{\rm cusp} = 1.8 \times 10^6$ at 3.8 yr to merger. Afterward, the source is entirely outside the caustic, producing four magnification peaks per orbit. The peak brightness decreases further as the binary approaches the merger. However, the minimum brightness increases, approaching the magnification of the single source lens at merger, in this case $\mu = 8 \times 10^4$, see Eq. (D7) in Supplemental Material [47].

Gravitational waves from such massive binaries can be observed by pulsar timing arrays: an inspiraling $2 \times 10^{10}M_\odot$ system is coincidentally detectable to $z \lesssim 0.3$ by NANOGrav 11 yr and to very high redshift with future data (Ref. [72], Fig. 4). Moreover, imposing a prior on the source position based on the QPLS detection increases the sensitivity with respect to all-sky GW searches [73].

(2) Eccentric binaries and space-borne GW detectors. Let us now consider the synergy between high-magnification lightcurves and milli-Hz GW detectors, such as LISA and TianQin. These observatories are sensitive to systems with total mass $\lesssim 10^8 M_\odot$.

Figure 3 shows three representative QPLS lightcurves for SMBHBs in the LISA and TianQin mass range starting at (0.75 Myr, 11 yr, 1.2 yr) before merger with initial

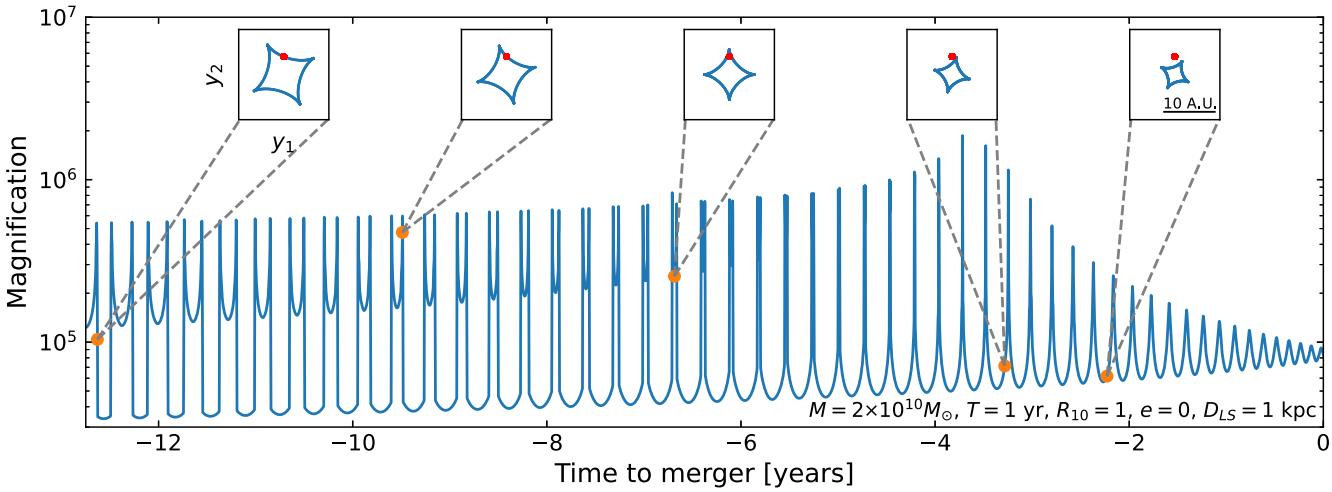


FIG. 2. Magnification as a function of time-to-merger in QPLS by an inspiraling $10^{10}M_\odot + 10^{10}M_\odot$ SMBH binary. The source star has a radius of $10R_\odot$ and is 1 kpc from the binary, the initial binary period is 1 year producing a lensing spike every 2 months. The host galaxy is assumed to be at redshift $z = 0.5$. The insets show the snapshots of the source plane with the fixed source star and the caustic curve, which rotates and shrinks during the inspiral. The source planes are plotted with the same scale shown in the last inset. Animations of the evolution of the SMBHB orbits, critical curves, images, caustic curves, and the lightcurve are demonstrated in a GitHub repository [71].

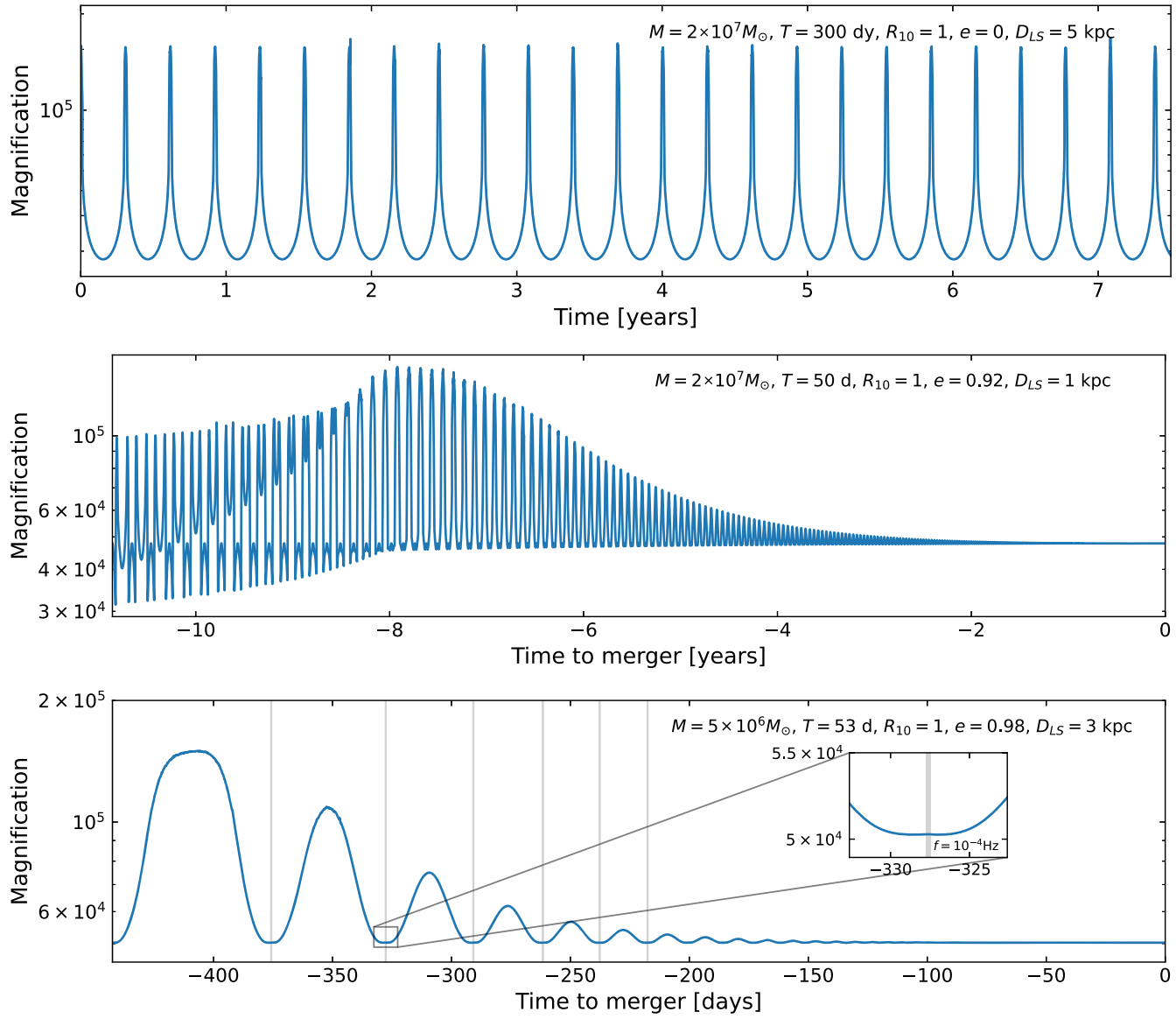


FIG. 3. Lensing lightcurves by SMBH binaries in the LISA mass range. The host galaxies are assumed to be at redshift $z = 0.5$. The total mass, initial period, initial eccentricity, source radius, and source-lens distance are labeled in the plots, where $T_{\rm day} = T/{\rm day}$. Top: a quasicircular LISA binary 7.5×10^5 yr before merger representing the LISA binary population at an earlier stage. Middle: an eccentric binary 11 years before merging in the LISA band. Bottom: a highly eccentric LISA binary that enters the LISA band during each periastron passage represented by the grey lines. The inset shows one periastron passage, where the width of the gray line represents the few hours long time interval where the gravitational wave bursts are in the LISA band [71].

eccentricity (0, 0.92, 0.98), respectively (see the legend for other parameters). These EM sources can inform the GW detection rate at a population level, provide an advance warning for future GW detections, and represent coincident multimessenger observations in the three cases, respectively. In the top panel, caustic crossing produces a periodic magnification in the early inspiral phase of the SMBHB population.

Early warning: In the middle panel, the caustic curve initially crosses the source during apocenter passages. Because of the varying size of the caustic curve, there is only one instance of caustic crossing during each period. As the orbit and the eccentricity shrink, the lightcurve initially exibits doubly peaked fold crossing, which then changes to a single-peaked cusp crossing and the modulation amplitude decays as the caustic shrinks and the source is fully outside of the caustic. For this system, the SMBHB enters the LISA band a few years after prominent QPLS modulation. The GW frequency peaks at 0.1 (0.02) mHz 0.8 days (5.5 months) before merger at which point the eccentricity is down to 0.05 (0.45).

Coincident multimessenger: the bottom panel shows the case of a highly eccentric $e = 0.98$ SMBHB lens being a LISA GW-source, where QPLS magnificantion peaks are initially again near the apocenter. In this case, the GW bursts emitted during pericenter passages (troughs of the EM lensing light curve) are already in the detectable frequency band (see inset and gray vertical lines) one year before merger. The LISA signal-to-noise ratio (SNR) for a single burst at pericenter reaches 10 at a cosmological redshift of $z \approx 0.5$ [74]. The LISA SNR accumulates mainly in the last months before merger; it reaches 10 at $z \approx 4.9$ (see Supplemental Material [47] for more details).

More details on multimessenger prospects and the parameter space of SMBHBs are given in End Matter.

Conclusions and prospects—We have described QPLS: how a slowly moving bright star lensed by a SMBHB imprints a modulation of the light-curve at the center of the host galaxy, offering a direct probe of the binary's orbit and its evolution. The lensing of individual bright stars results in spectacularly bright EM sources comparable to that of AGN even if the SMBHB lens resides in a quiescent galactic nucleus, in some cases outshining the light of the entire host galaxy. The QPLS light curve is a result of a combination of the binary orbit and the source's motion. Valuable information is contained in the separation between peaks, and width or amplitude of each peak, which is absent in many other transients. The spectrum (e.g. emission and absorption lines) of the source can also be used to distinguish lensed stars from other transients. (A spectral followup of the following peak(s) could be useful to identify a change in the spectral signature during the caustic crossing to reveal prominent stellar emission and absorption lines of the lensed starlight that were weaker before or after.) Very massive or eccentric SMBHBs can be also studied via GWs (PTAs or space detectors), either concurrently with QPLS or a few months or years after if the EM lightcurve provides an advance warning of the merger. This type of observation will enable "classical" multimessenger applications, including host identification, cosmography [75], and tests of general relativity [76]. QPLS lightcurves may also reveal tight SMBHBs also at an earlier evolutionary stage even without any GW detections.

Rapid developments in transient astronomy provide abundant opportunities to search for SMBHBs in this way: Zwicky Transient Facility observes variability over scales of minutes–years [77], Subaru's Hyper-Supreme Cam can preform targeted searches with cadence of minutes [78,79]. The Rubin Observatory will monitor $\sim 2 \times 10^{10}$ galaxies over ten years [80,81], with time resolution ~days (single filter). The Roman Space Telescope will search the sky with a smaller survey area but higher resolution and deeper imaging [82]. It is able to observe periodic signals of SMBHB with a cadence as low as 5 days to a depth of ~26 mag [83]. ULTRASAT will monitor ultraviolet variable events on scale of minutes to months [84]. In addition to wide-field seaches, further sensitivity to SMBHs can be achieved by dedicated observations of candidate systems.

The probability of a QPLS in a SMBHB can be estimated as the integral of the source density over the cylinder encompassing the central caustic, weighted by the probability of the source to remain within the caustic for at least an orbital period. Assuming a Gaussian velocity distribution and choosing a minimum $D_{\rm LS}$ such that $\xi_0 \geq a$ gives $P_{\rm QPLS} \sim 1.5 \times 10^{-5} \left(n_\star/{\rm pc}^{-3}\right) T_{\rm yr}^{8/3} M_{10}^{1/3} F_Q$, where the stellar density $n_\star$ is considered homogeneous and F_Q is a logarithmic correction that depends on M, T (see Supplemental Material [47] for more details). Extrapolating these rates to synthetic SMBHB catalogs [85] gives 1–50 $[190–5000]\left(n_\star/{\rm pc}^{-3}\right)$ QPLS sources in systems with a period below 10[40] yr (observer frame) at $z < 0.3$. These rates consider only comparable-mass systems $M_2/M > 0.5$, a rather small fraction of the total.

The presence of SMBHBs can be inferred from stars crossing the binary's caustic network, even for binaries with long period $T \gg 10$ yr or with stars that are too fast for multiple crossings due to orbit. For an individual SMBHB, the caustic crossing rate is 1.9×10^{-4} yr$^{-1} M_{10}^{1/3} T_{\rm yr}^{5/3} \left(n_\star/{\rm pc}^3\right) F_1$, where $F_1(\tilde{D}, M, T)$ is a logarithmic correction. (See Supplemental Material [47] for more details, including crossings of secondary caustics.) Extending this estimate to synthetic SMBHB populations [85], we find a total rate of $300 - 10^5 \left(n_\star/{\rm pc}^{-3}\right)$ [yr^{-1}] caustic crossings per year in all galaxies within $z < 0.3$. The rates includes only comparable-mass SMBHBs $M_2/M > 0.5$ at separations less than $10^3 GM/c^2$; the rates increase greatly when including wider separations, higher redshifts, or more asymmetric binary masses (see Supplemental Material [47] for more details). Considering only SMBHB populations in agreement with the high-z quasar luminosity function leads to rates $\geq 10^4 \left(n_\star/{\rm pc}^{-3}\right)$ yr^{-1}. These estimates warrant a more detailed analysis of the impact of SMBHB astrophysics, stellar population, and the sensitivity of time-domain surveys.

Realistic QPLS lightcurves require including additional effects, such as combining the peculiar motion of the star with the orbit of the SMBHB. Observing the lensing lightcurve will be easiest if the SMBHB lens is not embedded in gas. Gas around the SMBHB may lead to additional signatures: opaque regions may block some but possibly not all of the source's images as they move around the critical curve, potentially providing information on the size and structure of accretion disks. Indeed, there are typically two to four highly magnified images separated by 1.4 pc$M_{10}^{1/2} D_{\rm kpc}^{1/2}$ [Eq. (1)]. QPLS is also sensitive to other properties of SMBHBs, such as the mass ratio, and may be able to indicate the presence of a third SMBH. The tendency of luminous stars to form clusters provides

additional challenges and opportunities: i.e., multiple sources may need to be modeled but they may also probe the spatial structure of the lens. These effects may help distinguish SMBHBs lensing imprints from other processes that induce variability in a galaxy's lightcurve.

The high magnification and persistence of QPLS modulations may allow even moderately luminous stars to reveal SMBHBs. Even a Sun-like star $(1L_\odot, 1R_\odot)$ magnified by the SMBHB system similar to that in Fig. 2 but with arbitrary mass may be detectable by Rubin-legacy survey of space and time (LSST) (Roman) at a distance $\lesssim 80(400) M_{10}^{5/24} T_{\rm yr}^{-1/3} (R_{10}/0.1)^{-1/4} (L/L_\odot)^{1/2} D_{\rm kpc}^{3/8}$ Mpc [based on single exposure sensitivity of 24 (27.63) mag at 750 nm and Eq. (54) in the Supplemental Material [47]]. Photometric errors scale with the number of visits as $\propto 0.0082 \sigma_{m,\rm single} \sqrt{1\ \rm yr/t_{obs}}$, and can be further improved by knowing the lightcurve: matched filter techniques, similar to searches for GWs, may be used to recover QPLS signals from noise-dominated data. Additional gains may follow from spatial information (e.g., from pixel-level microlensing [86–88]) and spectral features, in addition to photometry, and from targeting galaxies more likely to harbor SMBHBs with very large telescopes. These and other advances in observations and data analysis will allow QPLS to open a new window to illuminate the most extreme objects in the heart of distant galaxies.

Acknowledgments—We acknowledge valuable discussions with Bruce Allen, Enrico Barausse, Jonathan Gair, Juan Garcia-Bellido, Graham Smith, and Stephen Taylor. This work was supported by the Science and Technology Facilities Council Grant No. ST/W000903/1 (to B. K.).

Data availability—The data that support the findings of this article are openly available [48,49,50,51,52].

[1] M. C. Begelman, R. D. Blandford, and M. J. Rees, Nature (London) **287**, 307 (1980).
[2] A. Escala, R. B. Larson, P. S. Coppi, and D. Mardones, Astrophys. J. **607**, 765 (2004).
[3] M. Volonteri, Astron. Astrophys. Rev. **18**, 279 (2010).
[4] M. Milosavljevic and D. Merritt, Astrophys. J. **596**, 860 (2003).
[5] P. A. Seoane *et al.* (LISA Collaboration), Living Rev. Relativity **26**, 2 (2023).
[6] M. Volonteri, F. Haardt, and P. Madau, Astrophys. J. **582**, 559 (2003).
[7] J. Kormendy and L. C. Ho, Annu. Rev. Astron. Astrophys. **51**, 511 (2013).
[8] G. Alonso-Álvarez, J. M. Cline, and C. Dewar, Phys. Rev. Lett. **133**, 021401 (2024).
[9] B. Kocsis, Z. Haiman, and K. Menou, Astrophys. J. **684**, 870 (2008).
[10] A. De Rosa *et al.*, New Astron. Rev. **86**, 101525 (2019).
[11] D. J. D'Orazio and M. Charisi, arXiv:2310.16896.
[12] T. Bogdanovic, M. C. Miller, and L. Blecha, Living Rev. Relativity **25**, 3 (2022).
[13] M. Charisi, S. R. Taylor, J. Runnoe, T. Bogdanovic, and J. R. Trump, Mon. Not. R. Astron. Soc. **510**, 5929 (2022).
[14] G. Agazie *et al.* (NANOGrav Collaboration), Astrophys. J. Lett. **951**, L8 (2023).
[15] J. Antoniadis *et al.* (EPTA and InPTA Collaborations), Astron. Astrophys. **678**, A50 (2023).
[16] D. J. Reardon *et al.* (PPTA Collaboration), Astrophys. J. Lett. **951**, L6 (2023).
[17] H. Xu *et al.*, Res. Astron. Astrophys. **23**, 075024 (2023).
[18] J. Ellis, M. Fairbairn, G. Hütsi, J. Raidal, J. Urrutia, V. Vaskonen, and H. Veermäe, Phys. Rev. D **109**, L021302 (2024).
[19] G. Sato-Polito, M. Zaldarriaga, and E. Quataert, Phys. Rev. D **112**, 123018 (2025).
[20] P. Amaro-Seoane *et al.*, arXiv:1702.00786.
[21] M. Colpi *et al.*, arXiv:2402.07571.
[22] J. Luo *et al.* (TianQin Collaboration), Classical Quantum Gravity **33**, 035010 (2016).
[23] J. Luo *et al.*, Classical Quantum Gravity **42**, 173001 (2025).
[24] P. Auclair *et al.*, Living Rev. Relativity **26**, 5 (2023).
[25] Z. Haiman, B. Kocsis, and K. Menou, Astrophys. J. **700**, 1952 (2009).
[26] D. J. D'Orazio, Z. Haiman, and D. Schiminovich, Nature (London) **525**, 351 (2015).
[27] M. Charisi, Z. Haiman, D. Schiminovich, and D. J. D'Orazio, Mon. Not. R. Astron. Soc. **476**, 461 (2018).
[28] C. Xin, M. Charisi, Z. Haiman, D. Schiminovich, M. J. Graham, D. Stern, and D. J. D'Orazio, Mon. Not. R. Astron. Soc. **489**, 819 (2019).
[29] Z. Song, J. Ge, Y. Lu, and X. Ji, Mon. Not. R. Astron. Soc. **493**, 588 (2020).
[30] P. Schneider, J. Ehlers, and E. E. Falco, *Gravitational Lenses* (Springer, Berlin, Heidelberg, 1992).
[31] V. Bozza, Gen. Relativ. Gravit. **42**, 2269 (2010).
[32] D. J. D'Orazio and R. Di Stefano, Mon. Not. R. Astron. Soc. **474**, 2975 (2018).
[33] J. Davelaar and Z. Haiman, Phys. Rev. Lett. **128**, 191101 (2022).
[34] L. Z. Kelley, D. J. D'Orazio, and R. Di Stefano, Mon. Not. R. Astron. Soc. **508**, 2524 (2021).
[35] L. M. Krauth, J. Davelaar, Z. Haiman, J. R. Westernacher-Schneider, J. Zrake, and A. MacFadyen, Phys. Rev. D **109**, 103014 (2024).
[36] D. L. Król, L. Stawarz, J. Krzesinski, and C. C. Cheung, Astrophys. J. **943**, 171 (2023).
[37] N. Li, S. Mao, L. Gao, A. Loeb, and R. Di Stefano, Mon. Not. R. Astron. Soc. **419**, 2424 (2012).
[38] Y. D. Hezaveh, P. J. Marshall, and R. D. Blandford, Astrophys. J. Lett. **799**, L22 (2015).
[39] S. Mao and B. Paczynski, Astrophys. J. Lett. **374**, L37 (1991).
[40] A. Gould and A. Loeb, Astrophys. J. **396**, 104 (1992).
[41] B. S. Gaudi, Annu. Rev. Astron. Astrophys. **50**, 411 (2012).
[42] J. Miralda-Escude, Astrophys. J. **379**, 94 (1991).
[43] P. L. Kelly *et al.*, Nat. Astron. **2**, 334 (2018).
[44] J. M. Diego, Astron. Astrophys. **625**, A84 (2019).

[45] G. Kauffmann, T. M. Heckman, C. Tremonti, J. Brinchmann, S. Charlot, S. D. M. White, S. E. Ridgway, J. Brinkmann, M. Fukugita, P. B. Hall, Ž. Ivezić, G. T. Richards, and D. P. Schneider, Mon. Not. R. Astron. Soc. **346**, 1055 (2003).

[46] P. Schneider and A. Weiss, Astron. Astrophys. **164**, 237 (1986).

[47] See Supplemental Material at http://link.aps.org/supplemental/10.1103/1sfl-87t4, Sec. A for details on methods and assumptions used when computing the magnification of the binary lens equation, which includes Refs. [48–56]; Sec. B for details on the topology and size of the caustic curves, which includes Ref. [57]; Sec. C for details on computing the magnification of an extended source near the caustic curve of a binary lens, which includes Ref. [58]; Sec. D for details on the magnification estimate at the trough and near merger for the lensing light curve, which includes Ref. [59]; Sec. F for details on the time duration estimate of caustic crossing; Sec. H for details on detection thresholds, which includes Refs. [60–62]; Sec. I for details on the GW-driven evolution of the binary and the detectability of the GWs of eccentric binaries, which includes Refs. [63–67]; Sec. J for details on the QPLS and caustic crossing rates, which includes Refs. [68,69]; and Sec. K for the special case of multiple QPLS sources.

[48] P. F. Hopkins, N. Murray, E. Quataert, and T. A. Thompson, Mon. Not. R. Astron. Soc. **401**, L19 (2010).

[49] J. M. Diego *et al.*, Astrophys. J. **857**, 25 (2018).

[50] M. Oguri, J. M. Diego, N. Kaiser, P. L. Kelly, and T. Broadhurst, Phys. Rev. D **97**, 023518 (2018).

[51] T. Venumadhav, L. Dai, and J. Miralda-Escudé, Astrophys. J. **850**, 49 (2017).

[52] C. V. Müller and J. Miralda-Escudé, Mon. Not. R. Astron. Soc. **536**, 1579 (2024).

[53] H. Erdl and P. Schneider, Astron. Astrophys. **268**, 453 (1993).

[54] M. Meneghetti, *Introduction to Gravitational Lensing: With Python Examples* (Springer, Cham, 2022).

[55] V. Bozza, Mon. Not. R. Astron. Soc. **408**, 2188 (2010).

[56] V. Bozza, E. Khalouei, and E. Bachelet, Mon. Not. R. Astron. Soc. **505**, 126 (2021).

[57] V. Bozza, Astron. Astrophys. **359**, 1 (2000).

[58] A. O. Petters, H. Levine, and J. Wambsganss, *Singularity Theory and Gravitational Lensing* (Birkhäuser, Boston, MA, 2001).

[59] O. Pejcha and D. Heyrovský, Astrophys. J. **690**, 1772 (2009).

[60] E. C. Bellm *et al.*, Publ. Astron. Soc. Pac. **131**, 018002 (2019).

[61] F. B. Bianco *et al.*, Astrophys. J. Suppl. Ser. **258**, 1 (2022).

[62] NASA Roman Science Team, Wide field instrument technical information, https://roman.gsfc.nasa.gov/science/WFI_technical.html (2024) (accessed: April 14, 2025).

[63] L. Barack *et al.*, Classical Quantum Gravity **36**, 143001 (2019).

[64] I. Mandel, Res. Not. Am. Astron. Soc. **5**, 223 (2021).

[65] S. Babak, M. Hewitson, and A. Petiteau, arXiv:2108.01167.

[66] T. Wagg, K. Breivik, and S. E. de Mink, Astrophys. J. Suppl. Ser. **260**, 52 (2022).

[67] T. Wagg, K. Breivik, and S. de Mink, J. Open Source Software **7**, 3998 (2022).

[68] M. T. Penny, E. Kerins, and S. Mao, Mon. Not. R. Astron. Soc. **417**, 2216 (2011).

[69] D. Merritt, Astrophys. J. **648**, 976 (2006).

[70] NASA/ESA Hubble Space Telescope, SXS Lensing/Max Planck Institute for Gravitational Physics, and P. Kervella (ESO). Composite figure including NGC 4414, colliding black holes simulation, and O-type star illustration, NGC 4414, Colliding black holes, O-type star (2025), images used under Creative Commons licenses: NGC 4414 image by NASA/ESA, CC BY 3.0; black hole simulation by SXS Lensing/Max Planck Institute for Gravitational Physics, CC BY 4.0; O-type star illustration by P. Kervella (ESO), CC BY-SA 3.0.

[71] https://github.com/whanxi/SMBHB-Lensing-Animations.

[72] A. R. Kaiser and S. T. McWilliams, Classical Quantum Gravity **38**, 055009 (2021).

[73] Z. Arzoumanian *et al.* (NANOGrav Collaboration), Astrophys. J. **914**, 121 (2021).

[74] Z. Xuan, S. Naoz, B. Kocsis, and E. Michaely, Astrophys. J. **965**, 148 (2024).

[75] B. F. Schutz, Nature (London) **323**, 310 (1986).

[76] E. Belgacem *et al.*, J. Cosmol. Astropart. Phys. 07 (2019) 024.

[77] M. J. Graham *et al.*, Publ. Astron. Soc. Pac. **131**, 078001 (2019).

[78] S. Miyazaki *et al.*, Publ. Astron. Soc. Jpn. **70**, S1 (2018).

[79] H. Aihara *et al.*, Publ. Astron. Soc. Jpn. **70**, S4 (2018).

[80] Ž. Ivezić *et al.*, Astrophys. J. **873**, 111 (2019).

[81] P. A. Abell *et al.*, arXiv:0912.0201.

[82] NASA Goddard Space Flight Center, Nancy Grace Roman Space Telescope, https://roman.gsfc.nasa.gov/index.html (2025) (accessed: April 22, 2025).

[83] Z. Haiman *et al.*, arXiv:2306.14990.

[84] Y. Shvartzvald *et al.*, Astrophys. J. **964**, 74 (2024).

[85] E. Barausse, K. Dey, M. Crisostomi, A. Panayada, S. Marsat, and S. Basak, Phys. Rev. D **108**, 103034 (2023).

[86] A. P. S. Crotts, Astrophys. J. Lett. **399**, L43 (1992).

[87] G. F. Lewis and R. A. Ibata, Astrophys. J. **549**, 46 (2001).

[88] R. Gil-Merino and G. F. Lewis, Astrophys. J. **643**, 260 (2006).

[89] P. C. Peters, Phys. Rev. **136**, 1224 (1964).

[90] S. J. Aarseth, IAU Symp. **246**, 437 (2008).

[91] A. Sesana, F. Haardt, and P. Madau, Astrophys. J. **686**, 432 (2008).

[92] I. Berentzen, M. Preto, P. Berczik, D. Merritt, and R. Spurzem, Astrophys. J. **695**, 455 (2009).

[93] M. Iwasawa, S. An, T. Matsubayashi, Y. Funato, and J. Makino, Astrophys. J. Lett. **731**, L9 (2011).

[94] M. Bonetti, A. Rasskazov, A. Sesana, M. Dotti, F. Haardt, N. W. C. Leigh, M. Arca Sedda, G. Fragione, and E. Rossi, Mon. Not. R. Astron. Soc. **493**, L114 (2020).

[95] F. M. Khan and K. Holley-Bockelmann, Mon. Not. R. Astron. Soc. **508**, 1174 (2021).

[96] A. Mastrobuono-Battisti, P. Amaro Seoane, M. J. Fullana i Alfonso, C. Omarov, D. Yurin, M. Makukov, G. Omarova, and G. Ogiya, Astron. Astrophys. **693**, A22 (2025).

[97] A. Gualandris, F. M. Khan, E. Bortolas, M. Bonetti, A. Sesana, P. Berczik, and K. Holley-Bockelmann, Mon. Not. R. Astron. Soc. **511**, 4753 (2022).
[98] P. Goldreich and R. Sari, Astrophys. J. **585**, 1024 (2003).
[99] J. Cuadra, P. J. Armitage, R. D. Alexander, and M. C. Begelman, Mon. Not. R. Astron. Soc. **393**, 1423 (2009).
[100] A. A. C. Roedig, M. Dotti, A. Sesana, J. Cuadra, and M. Colpi, Mon. Not. R. Astron. Soc. **415**, 3033 (2011).
[101] M. Siwek, L. Z. Kelley, and L. Hernquist, Mon. Not. R. Astron. Soc. **534**, 2609 (2024).
[102] N. Chen, D. Mukherjee, T. Di Matteo, Y. Ni, S. Bird, and R. Croft, Open J. Astrophys. **7**, 28 (2024).
[103] Y. Zhou, D. Mukherjee, N. Chen, T. Di Matteo, P. H. Johansson, A. Rantala, C. Partmann, U. N. Di Carlo, S. Bird, and Y. Ni, Astrophys. J. **980**, 79 (2025).
[104] D. Mukherjee, Y. Zhou, N. Chen, U. N. Di Carlo, and T. Di Matteo, Astrophys. J. **981**, 203 (2025).
[105] V. Manikantan, V. Paschalidis, and G. Bozzola, Astrophys. J. Lett. **984**, L47 (2025).

End Matter

In the End Matter, we discuss the synergy between QPLS lightcurves and space-borne GW detectors such as LISA and TianQin. We study the parameter space for which a multimessenger observation is possible, including both quasicircular and highly eccentric binaries.

Parameter space of multimessenger observations: Figure 4 summarizes the parameter space for multimessenger QPLS observations in terms of the SMBHB total mass and orbital period. Green, orange, and red lines correspond to sources merging in 10 years for different values of the initial eccentricity (0, 0.9, 0.99), respectively. Vertical/horizontal lines indicate the range of GW/EM facilities. The source presented in Fig. 2 is indicated with (A), and those in Fig. 3 are marked with (B)–(D), respectively. In many cases, caustic crossing of stars by SMBHBs observable by mHz GW detectors probe the same underlying population, but decades to millions of years before merger. Some of the most massive quasicircular LISA sources $(1+z)M \gtrsim 10^{7.5} M_\odot$ could represent delayed multimessenger events, where the lensing lightcurve arrives only a few years in advance, which can be detected by surveys such as Rubin-LSST, which has a cadence of ∼4 days (for a single filter) [80]. Indeed, the observed time to merger as a function of observed period for circular sources is $t_{\rm mg,c} = 8\ {\rm yr}(T_{20\ {\rm day}})^{-8/3} M_{8z}^{-5/3}[4q/(1+q)^2]^{-1}$ where q and $M_{8z} = (1+z)M/(2\times 10^8 M_\odot)$ represent the mass ratio and the redshifted total mass of the SMBHB, respectively [89].

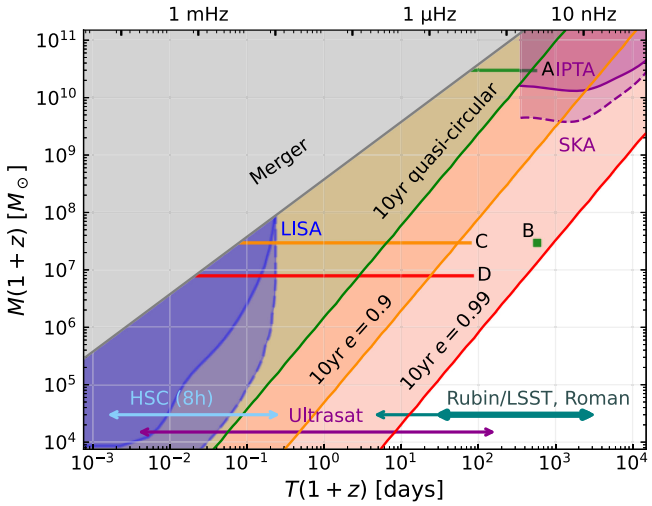


FIG. 4. Prospects for multimessenger observations of SMBHBs using QPLS in the plane of total SMBH mass and redshifted orbital period. Slanted filled regions show the systems that will merge in 10 years for different values of the eccentricity. Horizontal lines correspond to the systems shown in Figs. 2 (A) and 3 (B–D top to bottom) at $z = 0.5$. LISA regions show the orbital period where the signal-to-noise-ratio above 10^{-4} Hz reaches > 10 for equal-mass, nonspinning and quasicircular SMBHBs at $z = 0.5$ (dashed) and $z = 5$ (solid). PTA regions correspond to IPTA 2025 (solid) and SKA 2034 (dashed) for quasicircular q = 1 SMBHs at z = 0.5 [13]. Horizontal arrows show the cadence-to-survey time of several transient surveys (these apply for all masses). For Rubin/LSST we distinguish the cadence of any filter (thin, 4 days) from that of all six filters (thick, 24 days). A circular (eccentric) binary produces four (one) single-peaked or double-peaked caustic crossings during each orbital period.

Quasicircular binaries: For quasicircular SMBHBs, coincident detections of QPLS with mHz GWs requires not only high-cadence EM surveys (e.g., 30 min for Subaru HSC-SSP [79]), but also subsolar source diameters. Indeed, GW frequencies of $f_{\rm GW} \gtrsim 0.1$ mHz correspond to binary orbital periods of $T(1+z) = 1/(2f_{\rm GW}) \lesssim 4$ hr, the size of the caustic curve is smaller than $0.1 R_\odot M_{10}^{1/6} D_{\rm kpc}^{-1/2}$, and the magnification is suppressed for intrinsically larger $R_{\rm src}$ EM sources or for sources with smaller $D_{\rm LS}$ [see Eqs. (3)–(5)]. Detectable QPLS sources may be limited to the nuclear star cluster of the SMBHB lens for main sequence stars or else include the lensing of compact objects, such as white dwarfs, radio pulsars, or x-ray binaries. Bright inhomogeneities of larger sources (e.g., starspots or flares of O/B stars) may also be significantly magnified for circular SMBHBs emitting in the LISA band.

Highly eccentric binaries: Coincident EM and GW transients are easier to achieve for highly eccentric SMBHBs, as the merger time scales approximately as $t_{\rm mg,e} = (1-e^2)^{7/2} t_{\rm mg,c}$. This allows systems with total mass $\lesssim 10^7 M_\odot$ to evolve from $T \sim$ days (LSST cadence) to merger in a decade or less. There are multiple reasons to potentially expect eccentric SMBHBs. The scattering of

stars in the vicinity of the SMBHB [90–97] and/or the interaction with a gaseous disk [98–101] if present promotes eccentricity growth. Cosmological simulations followed by N-body simulations [102–104] also show evidence of a large number of merging massive binary systems with high eccentricity. The orbital eccentricity also leads to observable imprints on the QPLS lightcurve, as shown in the center and lower panels in Fig. 3. The binary separation becomes larger at apocenter passage, allowing for relatively larger stars to be highly magnified, compared to the quasicircular SMBHBs. The slow velocity at apocenter passage also increases the duration of each peak in the lightcurve. These factors make a coincident or delayed multimessenger observation more promising for an eccentric SMBHB. Similar effects of coincidental quasiperiodic GW and EM bursts are found in general relativistic magnetohydrodynamic simulations of eccentric SMBHBs with gas accretion [105]. This effect can be distinguished from QPLS by analyzing the spectrum.